ARTICLE

Raman Scattering at Resonant or Near-Resonant Conditions: A Generalized Short-Time Approximation

Abdelsalam Mohammed[a], Yu-Ping Sun[a,b], Quan Miao[a,c*], Hans Ågren[a], Faris Gel'mukhanov[a†]

a. Theoretical Chemistry, School of Biotechnology, Royal Institute of Technology, S-106 91 Stockholm, Sweden
b. School of Science, Shandong University of Technology, Zibo 255049, China
c. College of Physics and Electronics, Shandong Normal University, Ji'nan 250014, China

(Dated: Received on September 6, 2011; Accepted on September 9, 2011)

We investigate the dynamics of resonant Raman scattering in the course of the frequency detuning. The dephasing in the time domain makes the scattering fast when the photon energy is tuned from the absorption resonance. This makes frequency detuning to act as a camera shutter with a regulated scattering duration and provides a practical tool of controlling the scattering time in ordinary stationary measurements. The theory is applied to resonant Raman spectra of a couple of few-mode model systems and to *trans*-1,3,5-hexatriene and guanine-cytosine (G-C) Watson-Crick base pairs (DNA) molecules. Besides some particular physical effects, the regime of fast scattering leads to a simplification of the spectrum as well as to the scattering theory itself. Strong overtones appear in the Raman spectra when the photon frequency is tuned in the resonant region, while in the mode of fast scattering, the overtones are gradually quenched when the photon frequency is tuned more than one vibrational quantum below the first absorption resonance. The detuning from the resonant region thus leads to a strong purification of the Raman spectrum from the contamination by higher overtones and soft modes and purifies the spectrum also in terms of avoidance of dissociation and interfering fluorescence decay of the resonant state. This makes frequency detuning a very useful practical tool in the analysis of the resonant Raman spectra of complex systems and considerably improves the prospects for using the Raman effect for detection of foreign substances at ultra-low concentrations.

Key words: Resonant Raman, Scattering duration, Hexatriene, Short time approximation

I. INTRODUCTION

Operation of photon scattering at ultra-low intensities is most often required in order to apply Raman technique to detect single molecules or microscopic objects for which the basic cross sections are very small. Basically, only 10^{-7} of the photons incident on the sample material will undergo Raman scattering. The quality of the spectral fingerprint obtained for a molecular sample depends on several factors, such as the wavelength, linewidth and spectral purity of the excitation light, the extent to which the excitation or scattered light is absorbed, the amount of interfering fluorescence that is emitted, the potential existence of interfering laser-induced breakdown emission of materials and spectral congestion. Many variations of Raman spectroscopy have been developed in order to advantageously alter these factors and enhance the sensitivity. Perhaps the most cherished technique for that is surface enhanced Raman spectroscopy (SERS) [1, 2], which is based on the excitation of surface plasmons, or surface plasmon polaritons, by a metal surface, often nanostructured, which provides a very efficient way to couple energy into the sample.

When the frequency of the photon approaches the photoabsorption resonance the cross section of the scattering increases giving an 3 to 5 order of magnitude increase in sensitivity of the resonant Raman scattering (RRS). This extends the applicability of Raman detection in chemistry and material science, and for particular applications in the biomedical area like imaging of cells and molecules where most of the understanding about diseases is to be found. Other important applications include point detection of foreign substances in gaseous form or in interaction with substrates. However, the application of resonant conditions bears with it an increased risk of fluorescence and photo-degradation of the sample due to the increased energy of the incoming laser light. The analysis for the Raman signal in terms of molecular signatures and structure-to-property relations as the underlying descriptions then also be-

*Author to whom correspondence should be addressed. E-mail: qmiao@theochem.kth.se
†On leave from: Institute of Automation and Electrometry, Novosibirsk, Russia

DOI:10.1088/1674-0068/25/01/31-47

come more complex [3−17].

The sensitive and accurate detection of molecules at very low concentrations is thus still a challenge for Raman based techniques, even under resonant conditions. We are still in need of techniques enabling detection, identification and analysis of the smallest possible quantities of molecules in environments with minute amounts of the sample materials. One opportunity to improve the situation and to reach those goals is given by the the notion of "detuning" introduced in the context of resonant Raman scattering in the X-ray region [6], meaning that the laser frequency is tuned in steps away from the resonance. In order to realize the potential of this notion it is helpful to consider time-independent theory of RRS based on the Kramers-Heisenberg (KH) equation for the scattering cross section. This simple equation constitutes a main vehicle for calculations of RRS cross sections in molecules [6, 18−21] and solids [22] including electronic and nuclear degrees of freedom. This basic model takes into account the nuclear vibrations in the Born-Oppenheimer (BO) approximation, which reduces the calculation of the RRS amplitude to computation of the matrix elements of transition dipole moments between the vibrational wave functions.

The concept of detuning, however, better appeals to our intuition and understanding using a time-dependent picture, where it easily connects with notions such as "scattering time" and "fast" and "slow" scattering [4−6]. It rests on the fact that RRS is a dynamical process with the characteristic scattering duration [4−6, 23, 24] τ=$\tau(\Gamma,\Omega)$ which depends both on the lifetime broadening of intermediate electronic state Γ and on the detuning of the photon frequency from the absorption resonance Ω. The detuning of the frequency has practical applications as it lends a simple way to vary the duration of Raman scattering and to make it fast. This has been the basis for the prediction of several dynamical effects which subsequently have been experimentally observed in X-ray RRS. Important examples are collapse of vibrational structure [25], restoration of selection rules [4, 5], quenching of the atomic peak [21, 24], see review in Ref.[6]. These effects are observed when the nuclear wave packet promoted to the potential energy surface of the intermediate electronic state lacks time to spread because of the fast scattering. A motivation for the present work is to show that this notion is excellently applicable for Raman scattering also in the optical and ultraviolet (UV) spectral regions, and to the common situation when the the final and the ground electronic states coincide.

When the light promote the ground state nuclear wave packet in the excited state, this wave packet evolves in the potential surface of that state with a characteristic time equal to the vibrational period. This time is defined by the velocity of the fragments of dissociation if the excited state is unbound. In comparison, the RRS process has its own scale of time which depends on the homogeneous broadening and on the detuning of excitation frequency from the absorption resonance. Thus the dynamics of the resonant scattering is defined by the rivalry of these two characteristic times. The scattering is fast when the scattering duration is much shorter than the vibrational period, as in that case the nuclear wave packet lacks time to spread and revive undamaged. While, as noted above, the fast scattering is characterized by a set of interesting physical phenomena [4−6, 23, 24], it thus also brings about a great simplification of the theory.

The notion of fast scattering [4−6, 23, 24] has more recently been revived by Jensen and coworkers [7, 8], where the short-time (ST) approximation was introduced in the theory of RRS in the optical and UV regions. The mechanism of the shortening of the scattering duration suggested was, however, based solely on the characteristic time related to the homogeneous broadening Γ. We here refer to this approximation as the ST(Γ) short time approximation to make distinction from a more general shortening of the scattering here introduced and named ST(Γ,Ω).

The short time approximation involves the transitions with excitation/deexcitation of only one vibrational level, and requires therefore only the calculation of the first derivatives of the polarizability over normal coordinates [7, 8]. However, the ST(Γ) approximation overestimates the RRS cross section [26]. One should notice also the significant contribution of overtones and the RRS transitions with combinations of fundamental frequencies which are forbidden in this approximation. Indeed, experimental UV RRS data show strong overtones and combinatorial resonances for both small [27, 28] and larger molecules like *trans*-1,3,5-hexatriene, pyrene and anthracene and also for compounds like substituted pyrenes, adenosine monophosphate (AMP) and abietic acid. These features were demonstrated in early measurements [29, 30] and in more recent experimental studies [31]. The main reason for the mismatch is that the homogeneous broadening must exceed a few times the vibrational frequency to reach the short time limit in the resonant region. Analysis of available experimental data (see below) indicates that this is not the case in the optical and UV spectral regions, and even not in the soft X-ray region ($\omega\leq$3 keV) although the homogeneous broadening then is much larger [6].

We analyze the evolution of the RRS spectral shape in the course of shortening of the scattering duration [4−6, 23−25]. The general theory is applied to the RRS spectra of two qualitatively different systems; the guanine-cytosine (G-C) Watson-Crick base pair (DNA) and *trans*-1,3,5-hexatriene, as well as few-mode systems, in order to highlight important aspects. In particular, we outline in a one-mode model and a two-mode model system, with high and low frequencies modes, the regions of the detuning and of the homogeneous broadening where the RRS is fast. The latter molecule is representative of a case where the short-time approxi-

DOI:10.1088/1674-0068/25/01/31-47

mation in its original formulation [7, 8] is broken. We show that the shortening of the RRS duration by the detuning results in a considerable purification of the spectrum from higher overtones and low frequency modes. Since for large molecules the large number of resonances makes the RRS spectra appear as quite complex, the detuning gives a useful tool for simplification. We also analyse the region of applicability of the ST approximation (ST(Γ)) and show that it is approximately valid in the case of weak deviation of the excited state potential surface from the ground state one after a proper rescaling of the cross section.

II. THEORY

We study here a special case of resonant scattering when the photo-excitation of the molecule from the ground (0) to the electronic state (i) is followed by the emission of the final photon due to the spontaneous decay $i\rightarrow 0$ to the ground electronic state. The electronic transitions are accompanied by the excitations of the vibrational levels of the excited state ϵ_{ν_i} as well as the ground ϵ_ν state

$$\omega + |0,0\rangle \rightarrow |i,\nu_i\rangle \rightarrow \omega' + |0,\nu\rangle \tag{1}$$

The reason for this is the different potential energy surfaces of the ground state $E_0(Q)$ and excited $E_i(Q)$ state. Here ν_i and Q are truncated notations for the vector of the vibrational quantum numbers of all modes and of the vector of the normal coordinates, respectively.

Classical theory is unable to treat quantitatively a number of aspects of resonant light scattering, particular the frequency dependence, interference and selection rules. A quantum mechanical expression of the RRS cross section was given by Kramers and Heisenberg in 1925 [6, 32, 33].

$$\begin{aligned}\sigma(\omega,\varepsilon) &\equiv \frac{\mathrm{d}^2\sigma(\omega,\varepsilon)}{\mathrm{d}\omega'\mathrm{d}O'} \\ &= r_0^2\omega\omega'^3\sum_\nu |F_\nu|^2\Phi(\varepsilon-\epsilon_\nu+\epsilon_0)\end{aligned} \tag{2}$$

where $r_0{=}1/c^2{\approx}2.82$ fm is the Thomson radius, The initial and final photons are characterized, respectively, by the frequencies ω, ω' and polarization vectors $\mathbf{e}$, $\mathbf{e}'$, $\varepsilon{=}\omega-\omega'$ is the energy loss, $\Phi(\omega'-\omega)$ is the normalized spectral distribution of the incident radiation. We use atomic units and short notation (Eq.(2)) for the double differential cross section. The temperature of the sample is assumed to be smaller than the vibrational one.

The scattering amplitude for the RRS process (Eq.(1)) is directly related to the polarizability tensor α_{nm}.

$$\begin{aligned}F_\nu &= \sum_{nm}\mathrm{e}'_n\alpha_{nm}\mathrm{e}_m \\ &= \sum_{\nu_i}\frac{\langle 0|D_{0i}|\nu_i\rangle\langle\nu_i|D'_{i0}|\nu\rangle}{\omega-\omega_{i0}-\epsilon_{\nu_i}+\epsilon_0+i\Gamma}\end{aligned} \tag{3}$$

here $D_{0i}{=}\mathbf{e}\cdot\mathbf{d}_{0i}$, $D'_{i0}{=}\mathbf{e}'\cdot\mathbf{d}_{i0}$, the dipole moment of electron transition $\mathbf{d}_{i0}$ depends on the normal coordinate Q, Γ is the homogeneous broadening of the transition $0{\rightarrow}i$, $\omega_{i0}{=}E_i{-}E_0$ is the frequency of the adiabatical $0{\rightarrow}i$ transition, $Q{=}0$ corresponds to the minimum of the ground state potential surface $E_0(Q)$. We use below the short notation $E_j{\equiv}E_j^{\min}(Q)$ and relative potential energy $\varepsilon_j(Q)$ which is equal to zero at the minimum ($\varepsilon_j^{\min}(Q)=0$):

$$E_j(Q) = E_j + \varepsilon_j(Q), \quad j=i,0 \tag{4}$$

The off-resonant term is omitted in the scattering amplitude, because it is small in this studied resonant scattering.

The theoretical treatment of Raman scattering may be approached in two distinct ways, namely using the time independent second order perturbation theory or by the way of solution of time dependent problem. Because the main purpose of our article is the dynamical aspect of RRS we outline the theory of RRS in the time domain.

A. Time-dependent theory of RRS

We study the scattering of photons from continuum wave light source. The conventional RRS is a process linear in the intensity of the light. Due to this linearity the total RRS probability ϖ is the probability averaged over all incident photons. This means that it is natural to start with the consideration of resonant scattering of a single photon. We should pay attention to important specifics of such scattering. In agreement with the uncertainty principle the wave function of a single photon is delocalized in the time domain, namely, the strength of the electric field of a single photon $\zeta{=}\sqrt{2\pi\omega}$ does not depend on the time [33]. The interaction time between the molecule and single photon is equal to infinity $[-\infty,t]$. In other words, the time of the photon absorption is unknown. Thus the scattering is going through a coherent superposition of excited states created at different times. We will show below that the interference of the scattering channels with different absorption instants t affects strongly the dynamics of the RRS process.

After this physical picture, we now turn to an analysis of the scattering dynamics. The probability of the resonant scattering ϖ per unit time can be calculated in different ways. The density matrix technique gives a natural definition of this quantity [34, 35]

$$\begin{aligned}\varpi = -2\Im\left[\rho_{fi}(t)\zeta' D'_{i0}\mathrm{e}^{-i\omega' t}\right] \rightarrow \\ -2\Im\left[\langle\psi_i(t)|\zeta' D'_{i0}|\psi_f(t)\rangle\mathrm{e}^{-i\omega' t}\right]\end{aligned} \tag{5}$$

as the probability of population of the final state due to the RRS process (Eq.(1)).

$$\dot\rho_{ff}(t) + \Gamma_f\rho_{ff}(t) = \varpi \tag{6}$$

DOI:10.1088/1674-0068/25/01/31-47

The term $\Gamma_f\rho_{ff}(t)$ describes the decrease of the final state population $\rho_{ff}(t)=\langle\psi_f(t)|\psi_f(t)\rangle$ because of the weak decay of the final vibrational levels with the rate Γ_f. Here $\zeta'=\sqrt{2\pi\omega'}$ is the strength of the electric field of the emitted photon, $\rho_{fi}(t)=\langle\psi_i(t)|\psi_f(t)\rangle$ is the off-diagonal element of the density matrix.

We now solve the time-dependent Schrödinger equation for the nuclear wave function of the excited state

$$\left[i\frac{\partial}{\partial t}-(h_i+E_i-i\Gamma)\right]|\psi_i(t)\rangle=\zeta D_{i0}\mathrm{e}^{-i(\omega+E_0+\varepsilon_0)t}|0\rangle \tag{7}$$

The right-hand side describes the radiative coupling between the ground and excited states. The nuclear hamiltonian

$$h_j=T+\varepsilon_j(Q),\quad j=i,0 \tag{8}$$

is the sum of the operator of kinetic energy T and relative potential energy $\varepsilon_j(Q)$. Solution of Eq.(7)

$$|\psi_i(t)\rangle = -i\mathrm{e}^{-i(\omega+E_0+\epsilon_0)t}\zeta|\psi_i^\infty\rangle \tag{9}$$

$$\begin{aligned}|\psi_i^\infty\rangle &= \int_0^\infty \mathrm{d}t_1\mathrm{e}^{(i\Omega-\Gamma)t_1}|\phi_i(t_1)\rangle\\ &= \int_0^\infty \mathrm{d}t_1\mathrm{e}^{-t_1/\tau}|\phi_i(t_1)\rangle\end{aligned} \tag{10}$$

shows that the electromagnetic field excites the molecule in a coherent superposition of vibrational states of the ith electronic state

$$\begin{aligned}|\phi_i(t)\rangle &= \mathrm{e}^{-i(h_i-\epsilon_0)t}D_{i0}|0\rangle\\ &= \sum_{\nu_i}\mathrm{e}^{-i(\epsilon_{\nu_i}-\epsilon_0)t}|\nu_i\rangle\langle\nu_i|D_{i0}|0\rangle\end{aligned} \tag{11}$$

At this point we make the important observation that the evolution of the wave packet in the excited state has a characteristic time. This complex time we coin as the scattering duration time [4–6, 23]

$$\tau=\frac{1}{\Gamma-i\Omega}=\Re\tau+i\Im\tau \tag{12}$$

which is a function of Γ and of the detuning $\Omega=\omega-\omega_{i0}$ relative to the frequency of the adiabatical transition ω_{i0}. We see that the duration time τ indeed serves to specify the time interval which gives the main contribution in the integral (Eq.(10)) and hence in the scattering process.

The time $t_1=t-t_{\mathrm{abs}}$ in Eq.(10) is the time relative to the instant of the photon absorption t_{abs}. Therefore, the integration over t_1 is nothing else than the integration over the instants of the absorption $t\geq t_{\mathrm{abs}}\geq-\infty$. Thus the integral in the expression for $|\psi_i^\infty\rangle$ (Eq.(10)) sums all interfering paths in the time domain which are going through the different instants of the absorption t_{abs}. This interference plays a crucial role for the destructive interference caused by the detuning Ω. The role of $\Re\tau$ and $\Im\tau$ on the the evolution of the wave packet in the excited state is qualitatively different. When the photon frequency is tuned near the resonance the detuning is small. In this case the propagation of the wave packet is restricted only because of the irreversible depopulation of the excited state: $\tau\approx\Re\tau\approx1/\Gamma$. The evolution of the wave packet is also restricted for times longer than $1/|\Omega|$ due to the quenching of the long term contribution $t>1/|\Omega|$ caused by the fast oscillations of the integrand of $|\psi_i^\infty\rangle$ (see Eq.(10)). Contrary to the irreversible decay, these oscillations are reversible in principle because they are independent of the depopulation of the excited state. The physical reason of these oscillations is found in the destructive interference of excitation channels with different instants of absorption t_{abs}.

We are ready now to find the wave function of the final state which obeys to the Schrödinger equation

$$\left[i\frac{\partial}{\partial t}-(h_0+E_0-i\Gamma_f)\right]|\psi_f(t)\rangle=\zeta' D'_{0i}\mathrm{e}^{i\omega' t}|\psi_i(t)\rangle \tag{13}$$

where the right-hand side describes the coupling between the excited and final states caused by spontaneous emission of the final photon. Similar to Eq.(9) we obtain

$$\begin{aligned}|\psi_f(t)\rangle &= -\mathrm{e}^{-i(-\omega'+\omega+E_0+\epsilon_0)t}\zeta'\zeta\cdot\\ &\quad\int_0^\infty \mathrm{e}^{i(\omega-\omega'+\epsilon_0)t'-\Gamma_f t'}|\phi_f(t)\rangle\mathrm{d}t'\\ |\phi_f(t)\rangle &= \mathrm{e}^{-ih_0t}D'_{0i}|\psi_i^\infty\rangle\end{aligned} \tag{14}$$

Inserting of $|\psi_i(t)\rangle$ (Eq.(10)) and $|\psi_f(t)\rangle$ (Eq.(14)) into Eq.(5) brings in the time-dependent representation of the RRS probability [18, 21].

$$\varpi=2(\zeta\zeta')^2\Re\int_0^\infty \mathrm{e}^{i(\varepsilon+\epsilon_0)t-\Gamma_f t}\sigma(t)\mathrm{d}t \tag{15}$$

which is a half-Fourier transform of the autocorrelation function

$$\begin{aligned}\sigma(t) &= \langle\phi_f(0)|\phi_f(t)\rangle\\ &= \langle\psi_i^\infty|D'_{i0}\mathrm{e}^{-ih_0t}D'_{0i}|\psi_i^\infty\rangle\end{aligned} \tag{16}$$

In order to obtain the RRS cross section, ϖ should be divided by the photon flux $J=c\approx137$ and multiplied by the density of the states of the emitted photon $\mathrm{d}^2\sigma(\omega,\varepsilon)=\frac{\varpi}{J}\frac{\mathrm{d}\mathbf{k}'}{(2\pi)^3}$, where $\mathbf{k}'$ is the momentum of the final photon) [18, 21].

$$\sigma(\omega,\varepsilon)=\frac{r_0^2\omega\omega'^3}{\pi}\Re\int_0^\infty \mathrm{d}t\exp(i[\varepsilon+\epsilon_0]t-\Gamma_f t)\sigma(t) \tag{17}$$

The lifetime broadening of the final vibrational state is very small and can be neglected, $\Gamma_f\to0$. The main

DOI:10.1088/1674-0068/25/01/31-47

reason of the broadening of the RRS resonance is the spectral width of the incident radiation γ. This means that the RRS cross section $\sigma(\omega',\varepsilon)$ should be convoluted with the normalized spectral function $\Phi(\omega-\omega')$, where ω is the carrier frequency [34]. The result of this convolution is straightforward

$$\sigma(\omega,\varepsilon)=\frac{{r_0}^2\omega{\omega'}^3}{\pi}\Re\int_0^\infty \mathrm{d}t\exp(i[\varepsilon+\epsilon_0]t)f(t)\sigma(t) \quad (18)$$

Here $f(t)=\int_{-\infty}^{\infty}\mathrm{d}\nu \mathrm{e}^{i\nu t}\Phi(\nu)$ is the Fourier transform of the spectral function, which is assumed in our simulations to be the gaussian

$$\Phi(\nu)=\frac{1}{\sqrt{\pi\gamma'}}\exp\left[-\left(\frac{\nu}{\gamma'}\right)^2\right] \quad (19)$$
$$\gamma'=\frac{\gamma}{\sqrt{\ln 2}}$$

In this case,

$$f(t)=\exp\left[-\left(\frac{t\gamma'}{2}\right)^2\right]$$

Here γ is the half width at half maximum (HWHM) of the spectral function. The normalization factor of $\Phi(\nu)$ is omitted in the numerical simulations outlined below, $(\pi\gamma')^{-1/2}\to 1$.

B. Fast scattering

Let us note that only the time domain $t_1\leq\tau$ is important in the integral of Eq.(9). We assume that the detuning Ω or lifetime Γ is sufficiently high to make the scattering faster than the period of vibration

$$|\tau|\omega_0=\frac{\omega_0}{\sqrt{\Omega^2+\Gamma^2}}\ll 1 \quad (20)$$

This allows to use the following short-time expansion of the exponent in Eq.(10)

$$\begin{aligned}|\phi_i(t)\rangle&=\sum_{\nu_i}|\nu_i\rangle\langle\nu_i|\mathrm{e}^{-i\epsilon_{\nu_i}t}D_{i0}\mathrm{e}^{i\epsilon_0 t}|0\rangle\\&=\mathrm{e}^{-ih_it}D_{i0}\mathrm{e}^{ih_0t}|0\rangle\\&\approx D_{i0}\mathrm{e}^{-ih_it}\mathrm{e}^{ih_0t}|0\rangle\end{aligned} \quad (21)$$

To focus on the main problem we neglect here the Q-dependence of the transition dipole moment. This is a rather good approximation for the studied resonant scattering (see also below). Keeping in mind the short-time limit one can use the Baker-Campbell-Haussdorf (BCH) formula $\mathrm{e}^{\mathrm{A}}\mathrm{e}^{\mathrm{B}}\approx\mathrm{e}^{\mathrm{A}+\mathrm{B}}\mathrm{e}^{[\mathrm{A},\mathrm{B}]/2}$ [36]:

$$\begin{aligned}\mathrm{e}^{-ih_it}\mathrm{e}^{ih_0t}&\approx\mathrm{e}^{-i(h_i-h_0)t}\mathrm{e}^{t^2[h_i,h_0]/2}\\&=\mathrm{e}^{-i[\varepsilon_i(Q)-\varepsilon_0(Q)]t}\left(1+\frac{t^2}{2}[h_i,h_0]+\cdots\right)\end{aligned} \quad (22)$$

Thus the wave packet Eq.(20) has the classical form with the precision $(|\tau|\omega_0)^2$

$$|\phi_i(t)\rangle=D_{i0}\mathrm{e}^{i[\varepsilon_0(Q)-\varepsilon_i(Q)]t}|0\rangle+O((|\tau|\omega_0)^2) \quad (23)$$

This means that the role of the nuclear dynamics in the excited state caused by the kinetic energy operator T is not important when the scattering is fast and the wave packet lacks time to spread in the excited potential surface. The quantum dynamics affects the wave packet evolution through the commutator $[h_i,h_0]$ starting from the quadratic term ($\propto t^2$) in Eq.(21). Let us discuss this in more detail using the time-independent picture.

III. FAST SCATTERING IN THE TIME-INDEPENDENT PICTURE

We have thus established that the RRS process has a scattering duration time τ (Eq.(11)) which is short either when Γ is large or when $|\Omega|$ is large. We now turn to the short time approximation. When $|\tau|$ is small it is natural to expand the scattering amplitude (Eq.(3)) in series over powers of τ (Eq.(11))

$$\begin{aligned}F_\nu&=-i\tau\sum_{\nu_i}\frac{\langle 0|D_{0i}|\nu_i\rangle\langle\nu_i|D'_{i0}|\nu\rangle}{1-i\tau(\epsilon_0-\epsilon_{\nu_i})}\\&=-i\tau\sum_{n=0}^{\infty}\sum_{\nu_i}(i\tau)^n\langle 0|D_{0i}(\epsilon_0-\epsilon_{\nu_i})^n|\nu_i\rangle\langle\nu_i|D'_{i0}|\nu\rangle\end{aligned} \quad (24)$$

Usually the Q-dependence of the transition dipole moments is weaker in comparison with $\varepsilon_j(Q)$. This allows to extract D_{0i} and D'_{i0} from the matrix elements. Before going further, we pay attention to the following approximate equation

$$\begin{aligned}\langle 0|(\epsilon_0-\epsilon_{\nu_i})^n|\nu_i\rangle&\approx\langle 0|(h_0-h_i)^n|\nu_i\rangle\\&=\langle 0|[\varepsilon_0(Q)-\varepsilon_i(Q)]^n|\nu_i\rangle\end{aligned} \quad (25)$$

which is strict for n=0 and n=1 since $h_j|\nu_j\rangle=\epsilon_{\nu_j}|\nu_j\rangle$. Eq.(25) is valid for $n\geq 2$ only in the classical limit

$$[h_0,h_i]=\{T,[\varepsilon_i(Q)-\varepsilon_0(Q)]\}\to 0 \quad (26)$$

Nevertheless, we will see below that conclusions based on Eq.(25) are valid even for $n\geq 2$ (higher overtones). Eq.(25) and the closure condition $\sum_{\nu_i}|\nu_i\rangle\langle\nu_i|=1$ lead to the following ST expansion of the RRS amplitude

$$\begin{aligned}F_\nu&\approx-i\tau D_{0i}D'_{i0}\sum_{n=0}^{\infty}(i\tau)^n\langle 0|[\varepsilon_0(Q)-\varepsilon_i(Q)]^n|\nu\rangle\\&\approx-i\tau D_{0i}D'_{i0}\big[\delta_{\nu,0}+i\tau\langle 0|\varepsilon_0(Q)-\varepsilon_i(Q)|\nu\rangle\\&\quad+O(\tau\omega_0)^2\big]\end{aligned} \quad (27)$$

When the scattering duration is short (Eq.(20)) the RRS vibrational profile collapses to the single (unshifted line):

$$F_\nu\approx\frac{D_{0i}D'_{i0}}{\Omega+i\Gamma}\delta_{\nu,0} \quad (28)$$

DOI:10.1088/1674-0068/25/01/31-47

This collapse effect predicted in Ref.[25] was observed for many systems in X-ray RRS [37−39] and resonant Auger scattering [6, 37]. The sum over n in Eq.(27) can be taken rigorously and we get the quantum scattering amplitude in the classical approximation (Eq.(26))

$$F_\nu \approx \langle 0|F(Q)|\nu\rangle \tag{29}$$

$$F(Q) = \frac{D_{0i}(Q)D'_{i0}(Q)}{\varepsilon_0(Q)-\varepsilon_i(Q)+i/\tau} = \frac{D_{0i}(Q)D'_{i0}(Q)}{\Omega+\varepsilon_0(Q)-\varepsilon_i(Q)+i\Gamma} \tag{30}$$

as the matrix element of the classical scattering amplitude $F(Q)$. We inserted here D_{0i} and D'_{i0} in the matrix elements again because the Q-dependence of $\varepsilon_i(Q)-\varepsilon_0(Q)$ is significantly strong, especially near the resonance. It is easy to see that the classical limit in the time dependent picture (Eqs.(29) and (30)) also results in Eqs.(29) and (30). This equation is strict only when the scattering is fast. It might here be tempting to use the classical scattering amplitude Eq.(29) even in the resonant region where the scattering is slow. However, numerical calculations show that the accuracy of Eqs.(29) and (30) is rather poor in the resonant region because the dynamical effects caused by T are neglected.

A. Small change of the potential energy surface upon electronic excitation

Instead of a convenient expansion of powers of Q, the ST expansion (Eq.(27)) runs over powers of $\varepsilon_i(Q)-\varepsilon_0(Q)$. The nonlinear dependence of $\varepsilon_i(Q)-\varepsilon_0(Q)$ on Q does not allow to reach certain conclusions about the number of overtones which are active in the RRS. This nonlinearity is strong when one of the vibrational modes is dissociative in the excited state [6, 39] or in the case of strong anharmonicity of the bound states. The latter case occurs quite often due to vibronic coupling; a typical example is a double-well potential of the excited state [40]. The nonlinearity can be strong even for harmonic potentials if the vibrational frequency significantly changes under excitation. For example

$$\varepsilon_0(Q) = \frac{\mu\omega_0^2 Q^2}{2} \tag{31}$$

$$\varepsilon_i(Q) = \frac{\mu\omega_i^2 (Q-\Delta Q)^2}{2} \tag{32}$$

$$\varepsilon_i(Q)-\varepsilon_0(Q) = \frac{\mu}{2}\left[Q^2(\omega_i^2-\omega_0^2)-2Q\omega_i^2\Delta Q+(\omega_i\Delta Q)^2\right] \tag{33}$$

which has both linear and quadratic dependencies on Q. Here ΔQ is the displacement of the potential of the excited state relative to the ground state equilibrium and μ is the reduced mass of this mode.

Nevertheless, the anharmonicity is quite often weak and the change of the vibrational frequency is not strong ($\omega_i \approx \omega_0$). In this case $\varepsilon_i(Q)-\varepsilon_0(Q)$ is a linear function of the normal coordinate Q

$$\varepsilon_i(Q)-\varepsilon_0(Q) \approx \omega'_{i0}Q + \frac{\mu}{2}(\omega_0\Delta Q)^2 \tag{34}$$

$$\omega'_{i0} = \frac{\partial[\varepsilon_i(Q)-\varepsilon_0(Q)]}{\partial Q} = \frac{-\omega_0\Delta Q}{a^2}, \quad Q=0 \tag{35}$$

Only in this case the short-time expansion (Eq.(24)) corresponds to the expansion of the scattering amplitude (Eq.(30)) or polarizability over powers of Q

$$F(Q) = \sum_{n=0}^{\infty}\frac{F^{(n)}}{n!}Q^n \approx -i\tau D_{0i}D'_{i0}\sum_{n=0}^{\infty}(-i\tau\omega'_{i0}Q)^n \tag{36}$$

The nth derivative $F^{(n)}$ of the classical scattering amplitude $F(Q)$ at Q=0 is calculated here by neglecting the weak dependence of the transition dipole moment on Q. In the case at hand ($|\tau|\omega_0 \ll 1$), the intensity of the νth overtone is more strongly suppressed for higher ν, because

$$F_\nu = \sum_{n=0}^{\infty}\frac{F^{(n)}}{n!}\langle 0|Q^n|\nu\rangle \approx \frac{1}{\nu!}F^{(\nu)}\langle 0|Q^\nu|\nu\rangle \approx \frac{a^\nu F^{(\nu)}}{\sqrt{2^\nu\nu!}} = -i\tau D_{0i}D'_{i0}(i\eta\tau\omega_0)^\nu\sqrt{\frac{\nu!}{2^\nu}} \tag{37}$$

here $a=1/\sqrt{\mu\omega_0}$ is the size of the vibrational wave function, $\Delta Q=-\omega'_{i0}a^2/\omega_0$ and $\eta=\Delta Q/a$ is the relative displacement which defines the FC amplitudes [41, 42]. Taking into account $\langle 0_0|Q|1_0\rangle = a/\sqrt{2}$, we get the following expression for the leading terms in the ST expansion:

$$F_0 = -i\tau D_{0i}D'_{i0} \tag{38}$$

$$F_1 = \frac{(-i\tau)^2 D_{0i}D'_{i0}a\omega'_{i0}}{\sqrt{2}} \tag{39}$$

Let us remind that the accuracy of Eq.(37) is rather poor for $\nu_f \geq 2$ where we used the classical approximation. However, we will see below that numerical calculations support our key conclusion concerning spectral narrowing of the RRS band due to a gradual quenching of higher overtones (ν=2, 3,$\cdots$) in the course of shortening of the scattering duration $|\tau|$. The relation $F_\nu \propto (\tau\omega_0)^\nu$ leads to another remarkable fact: the low frequency modes disappear faster from the RRS spectrum when the RRS duration decreases. Such a frequency selective purification of the spectrum by the increase of $|\Omega|$ should serve as a useful tool in assignments of spectra.

DOI:10.1088/1674-0068/25/01/31-47

The largest contribution to the RRS cross section (after the unshifted line ν=0) origins from ν=1 in the ST approximation (Eq.(20) and Eq.(37))

$$F_1^{\rm ST} \approx D_{0i} D'_{i0} \frac{\omega_0 \eta}{(\Omega + i\Gamma)^2} \frac{1}{\sqrt{2}} \tag{40}$$

We should now compare this result with the strict theory, which gives the same "selection" rules 0 →0,1 only when the potential changes only slightly under electronic excitation. This implies a small Huang-Rhys (HR) parameter

$$S = \eta^2 \ll 1 \tag{41}$$

One should notice that the HR parameter has the simple physical meaning of the vibrational quantum number near the vertical photoabsorption transition [43] when $S \gg 1$. Only 0-0-1 and 0-1-1 interfering channels contribute in strict RRS when the HR parameter is small

$$\begin{aligned} F_1 &\approx D_{0i} D'_{i0} \left(\frac{\langle 0|1_i\rangle\langle 1_i|1\rangle}{\Omega - \epsilon_{1_i} + \epsilon_0 + i\Gamma} + \frac{\langle 0|0_i\rangle\langle 0_i|1\rangle}{\Omega - \epsilon_{0_i} + \epsilon_0 + i\Gamma} \right) \\ &\approx D_{0i} D'_{i0} \left(\frac{1}{\Omega - \omega_0 + i\Gamma} - \frac{1}{\Omega + i\Gamma} \right) \frac{\eta}{\sqrt{2}} \end{aligned} \tag{42}$$

We would like to point out that the FC amplitudes $\langle 0|0_i\rangle \approx \langle 1_i|1\rangle \approx 1$ and $\langle 0|1_i\rangle \approx -\langle 0_i|1\rangle \approx \eta/\sqrt{2}$ differ qualitatively from the FC amplitude $\langle 0|Q|1\rangle = a/\sqrt{2}$ of the ST limit (Eq.(36)).

We study here RRS in the optical and UV regions. As already mentioned, the lifetime broadening of the related excited states of gas phase molecules is much smaller than the vibrational frequency

$$\Gamma \ll \omega_0 \tag{43}$$

This means that the ST limit (Eq.(20)) can be reached only by detuning from the absorption resonance. The comparison of Eqs.(40) and (42) indicates that the ST approximation breaks down in the resonant region. Indeed, the ST(Γ) approximation gives wrong dependence of the RRS profile on both the detuning and Γ. Nevertheless, simulations based on the ST(Γ) approximation are often in reasonable agreement with the experiment when the HR parameter is small (Eq.(41)). The reason for this is that both the ST(Γ) approximation and strict theory results in the same selection rules 0→0,1 when the change of nuclear potential upon excitation is weak Eq.(41). Nevertheless, the notion of the absorption resonance is ill defined in the ST(Γ) approximation and it is instructive to consider the ratio of the RRS peak intensities $|F_1/F_1^{\rm ST}|^2$ when the photon frequency is tuned in photoabsorption resonance with a certain vibrational level

$$\frac{\sigma(\omega,\varepsilon)}{\sigma_{\rm ST}(\omega,\varepsilon)} = \frac{\Gamma^2}{\omega_0^2} \to \frac{\Gamma^2}{\omega_{\alpha 0}^2} \tag{44}$$

This equation shows that the ST(Γ) approximation overestimates the cross section [26] and gives an incorrect RRS spectral shape because different vibrational modes have different frequencies $\omega_{\alpha 0}$. Eq.(37) gives a way to improve the ST(Γ) approximation by multiplying the peak intensity of the RRS cross section by the factor $\Gamma^2/\omega_{\alpha 0}^2$. The reason of the sensitivity of this rescaling factor to the vibrational frequency lies in the qualitatively different FC amplitudes of the ST(Γ) approximation and of the strict theory $\omega_{i0}^{(1)}\langle 0|Q|1_i\rangle/[\langle 0|1_i\rangle\langle 1_i|1\rangle] \approx \omega_{i0}^{(1)}\langle 0|Q|1_i\rangle/\langle 0|1_i\rangle = \omega_0$. The Γ can reach 0.01 eV or even 0.1 eV in the liquid phase. An additional reason for the disagreement exists in this case, namely the interference between vibrational levels of the excited state which is overestimated in the ST limit (Eq.(39)) due to the assumption about a large Γ.

To conclude, the applicability of the ST(Γ) approximation in the resonant region is limited to the cases $\Gamma \gg \omega_0$. Otherwise it results in an erroneous dependence of the RRS spectrum on Γ and frequency of the incoming light: $\sigma_{\rm ST} \propto 1/[(\omega-\omega_{i0})^2 + \Gamma^2]^2$ instead of $\sigma \propto 1/[(\omega-\omega_{i0})^2 + \Gamma^2]$, and results in incorrect absolute and relative peak RRS cross sections. Due to this one can not introduce a single correction factor to improve the short-time approximation.

IV. COMPUTATIONAL DETAILS

In the present study we select two molecules for illustrating our theory, namely the Watson–Crick DNA base pair methylguanine-methylcytosine (MG-MC) and *trans*-1,3,5-hexatriene (C_6H_8). The calculations of the Raman scattering cross sections are compared to experimental data obtained at room temperature of 300 K.

The underlying molecular property calculations are performed at the adiabatic DFT level of theory with the use of the correlation consistent basis sets of Dunning [44]. Calculations of force fields and polarizabilities are performed with the Dalton program [45]. Force fields are determined with use of the hybrid B3LYP exchange-correlation functional [46−49] in conjunction with the double-ζ basis set (cc-pVDZ) for base pairs DNA and triple-ζ basis set (cc-pVTZ) for THT. In addition to the B3LYP functional, also the Coulomb attenuated method B3LYP (CAM-B3LYP) functional [50] (with parameters α=0.19, β=0.46, and μ=0.33), and the double augmented basis sets d-aug-cc-pVDZ (for DNA) and d-aug-cc-pVTZ (for C_6H_8) are used in the calculations of polarizabilities and absorption spectra.

A common relaxation parameter of Γ=1000.0 cm^{-1} and Γ=64 cm^{-1} is used for the excited states for DNA and THT, respectively. The derivatives of both the polarizability tensor and the potential energy surface of the excited state with respect to nuclear displacements are determined at the equilibrium geometry and with the normal coordinates of the mentioned force fields.

DOI:10.1088/1674-0068/25/01/31-47

The numerical differentiations are performed along the mass-weighted normal coordinates Q with step lengths of $\pm 0.01\sqrt{\text{AMU}}$ a.u., where AMU≈1822.888.

In many articles [7, 8, 26] attention is paid only to one aspect of the scattering dynamics, namely to the lifetime of the intermediate electronic state. However, this is not correct even in the soft X-ray region because the lifetime of core-excited intermediate state $\tau \approx 1-10$ fs (the lifetime broadening ≤ 0.1 eV) is comparable with the vibrational period. Indeed, X-ray experiment as well as theory [4−6, 23−25] indicate strong transitions to higher excited vibrational states with the quantum numbers $\nu_f \geq 2,3$, *etc.*, which are forbidden in the ST(Γ) limit [7, 8]. We remind that even for large lifetime broadening (0.64 eV, $\tau \approx 1$ fs) of the intermediate state in X-ray RRS of HCl [39], the nuclear dynamics is very strong as well as the dependence of the scattering spectral profile on the detuning.

Apparently, the homogeneous broadening of optical or UV absorption profiles is much smaller than that in the X-ray region. Let us remind that the homogeneous broadening is a sum of the population decay rate $\Gamma_i/2$ and the dephasing rate γ_d: $\Gamma=\Gamma_i/2+\gamma_d$. The excited electronic state is depopulated through radiative and nonradiative decay channels. The nonradiative decay is faster than the radiative decay for higher excited states due to the internal conversion [51], with a characteristic time about 100−1000 fs in the optical and UV regions. For example, the analysis of the experimental data for the THT molecule [29] gives the following estimate Γ(HWHM)≈64 cm^{-1}=7.9 meV. The extensive analysis [52] of homogeneous broadening results in a rather similar value Γ=7.3 meV. The dephasing and environmental broadening are the main sources of the broadening in liquids. However, even in the liquid phase it is difficult to expect that Γ exceeds 0.1 eV. We will show below that the ST(Γ) limit in the resonant region can not be reached in real systems for $\Gamma \leq 0.1$ eV. The intense overtones seen in the RRS spectra of both gas and liquid phases directly evidence the break down of the ST(Γ) approximation [27−31], as a small value of Γ does not allow to use the ST(Γ) approximation. Instead, the regime of fast scattering can be reached by detuning of the frequency from resonance. Let us discuss this case in more detail.

V. RESULTS AND DISCUSSION

Let us start with the analysis of the fast scattering considering model systems. To give insight in the dynamics of the RRS we consider first the RRS of one- and two-mode model molecules.

A. Resonant Raman scattering by one-mode molecule

To exemplify the theory we consider the case of a single mode system when Δ_Q=0.2 a.u., ω_0=0.2 eV and μ=8AMU. The bandwidth of the incident light is chosen as γ=5 meV which is larger than the typical linewidth of the laser radiation. However, this does not affect the RRS profile because $\gamma \ll \omega_0$. The simulations shown in Fig.1 are performed for Γ=1 meV.

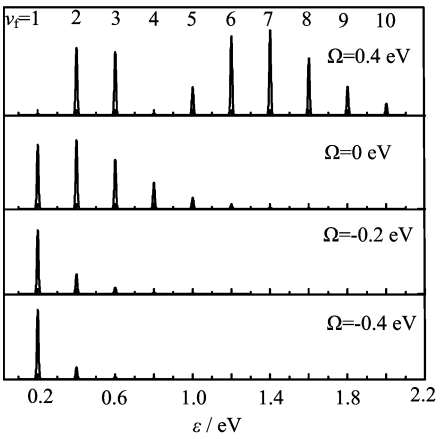

FIG. 1 The RRS spectrum for different detuning. One-mode model. Γ=1 meV, γ=5 meV.

The RRS profiles shown in Fig.1 and Fig.2 display strong dependence on both the detuning Ω and lifetime broadening Γ. When the photon energy is tuned in the region of strong photoabsorption, the main reason for sensitivity of the spectrum (Fig.1) on the detuning refers to the FC amplitudes $\langle\nu_f|\nu_i\rangle\langle\nu_i|0\rangle$. One can see quite many intense overtones ν_f=2−10 (Fig.1) when the photon frequency is tuned in resonance with the strongest absorption peak ν_i=2 (Ω=0.4 eV) (see Fig.3(b)) (slow scattering, $|\tau|\omega_0 \gg 1$). The highest overtones ν_f>5 are suppressed when the frequency is tuned to the relatively weak first absorption resonance (ν_f=0 (Ω=0)). The interference [6, 18] of the scattering channels through the different intermediate vibrational levels ν_i affects strongly the RRS profile when Ω is tuned between the vibrational resonances [53]. In agreement with the short time expansion (Eq.(36)), all overtones are gradually quenched when the photon frequency is tuned below the first resonance $\Omega < -\omega_0 = -0.2$ eV (Fig.1). In this region the scattering duration becomes shorter than the period of vibrations ($|\tau|\omega_0 \ll 1$). We already know that the scattering can be shortened by increasing Γ. The evolution of the RRS spectrum as a function of Γ displays the same effect, namely the suppression of higher overtones when Γ becomes larger than the vibrational frequency ω_0 (Fig.2).

The simulations of the RRS spectra (Fig.1 and Fig.2) show three distinct regions

$$|\tau|\omega_0 \gg 1, \quad |\tau|\omega_0 \approx 1, \quad |\tau|\omega_0 \ll 1 \tag{45}$$

When the scattering is long ($|\tau|\omega_0 \gg 1$) one can see extensive vibrational structure. The effect of lifetime-vibrational interference (LVI) [6, 18] is suppressed in this case. The shape of the profile changes when

DOI:10.1088/1674-0068/25/01/31-47

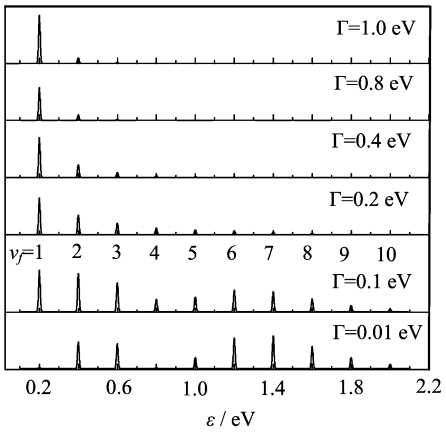

FIG. 2 The RRS spectrum for different lifetime broadenings of the intermediate electronic state. One-mode model. Ω=0.4 eV, γ=5 meV.

the RRS duration approaches the period of vibrations $|\tau|\omega_0 \approx 1$ and the LVI effect becomes large because of the interference between intermediate vibrational states. The overtones ($\nu_f > 1$) are quenched when the scattering becomes fast $|\tau|\omega_0 \ll 1$.

It is instructive to analyze the relative peak intensity of the overtones. Let us consider the rather typical situation of RRS of an almost monochromatic laser beam with $\gamma \ll \omega_0$. In this case the overlap of the nearby RRS peaks is negligibly small and the relative peak intensity of the ν_fth overtone reads

$$P_{\nu_f}(\Omega, \Gamma) = \frac{|F_{\nu_f}|^2}{|F_1|^2} \tag{46}$$

The calculations of $P_{\nu_f}(\Omega, \Gamma)$ versus Ω and Γ are depicted in Fig.3 and Fig.4 respectively. The main role of Γ is to increase the interference between the vibrational levels of the intermediate electronic state [6, 18]. This happens when the RRS duration Eq.(12) becomes sufficiently short Eq.(20). Figures 3 and 4 show that Γ and Ω affect differently the relative intensities of the overtones. The detuning is clearly related with scattering duration above and below the photoabsorption band. The simulations show that the scattering becomes fast when

$$\Omega \leq -\omega_0, \quad \Omega \geq \Delta, \quad \Gamma \geq \omega_0 \tag{47}$$

This condition of fast scattering (or the ST approximation) is more accurate than the previous one (Eq.(20)). One should mention that the main simulations in Fig.3 are performed for a rather large Γ=0.1 eV. The reason for this is only to avoid drawing too large values of P_{ν_f} between the resonances. As one can see from Fig.3, the decrease of Γ does not significantly affect the blue and red wings of P_{ν_f}. The results of simulations lead to the important conclusion that the short-time approximation in the sense of the articles in Refs.[7, 8] starts

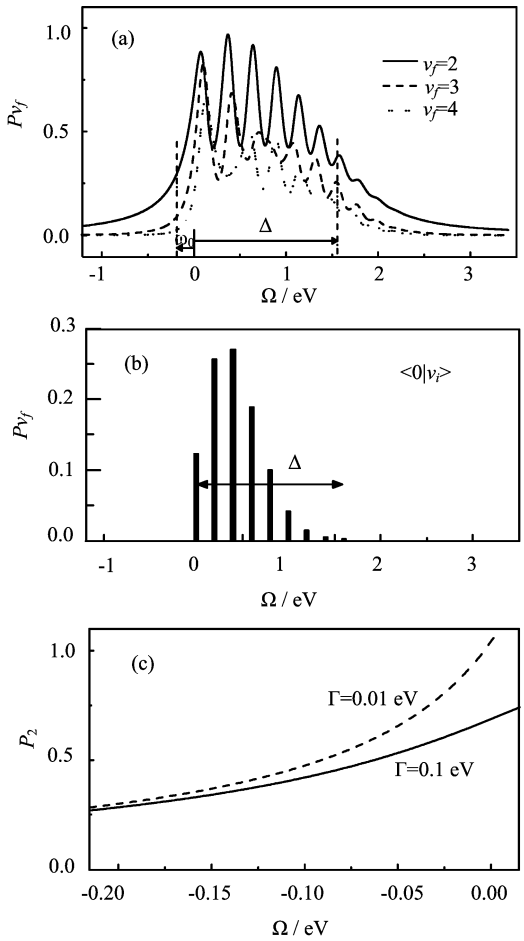

FIG. 3 Ratio of the peak intensities P_{ν_f} *vs.* the detuning Ω for Γ=0.1 eV and 0.01 eV. One-mode model.

to work for an unrealistically large Γ≫1 eV. However, one can reach the short-time limit easily by decreasing the detuning [6] (Fig.3).

B. Resonant Raman scattering by a two-mode molecule

Let us consider now the RRS spectrum of a molecule with two vibrational modes. The first mode has the vibrational frequency ω_{10}=0.2 eV while the second "soft" mode has much smaller frequency ω_{10}=0.06 eV. The relative shifts of the minima of the potential surfaces of the excited state are $\Delta Q_1/a_{10}$=2.07, $\Delta Q_2/a_{20}$=2.27, where $a_{\alpha 0}$ is the size of the vibrational wave function (ν_α=0) of the ground state. Figure 5 shows results of simulations for different detuning frequencies and lifetime broadenings. In an agreement with the analysis of the previous section (Eq.(47)) we see that the contribution of the soft mode is quenched faster than the peaks related to the high frequency mode when either the lifetime broadening increases or the detuning Ω decreases from the resonance (Fig.3). The shortening of the scattering duration using the variation of the detun-

DOI:10.1088/1674-0068/25/01/31-47

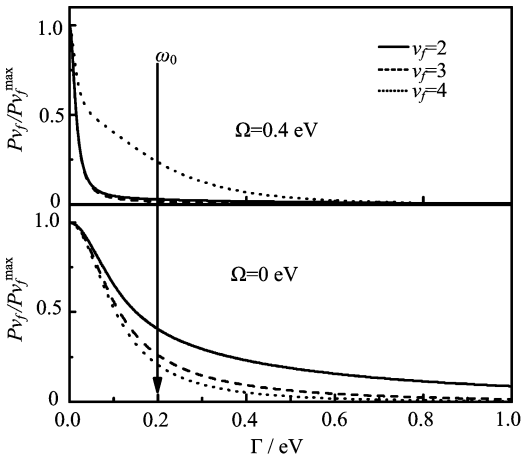

FIG. 4 The relative ratio of the cross sections $P_{\nu_f}/P_{\nu_f}^{\max}$ (Eq.(42)). One-mode model. The maximum of P_{ν_f} takes place at $\Gamma\to 0$. $P_{\nu_f}^{\max}=P_{\nu_f}(\Omega,0)$. $P_2^{\max}$=18.72 (1.05), $P_3^{\max}$=19.05 (0.73), $P_4^{\max}$=0.74 (0.39) for $\Omega=0.4(0)$ eV.

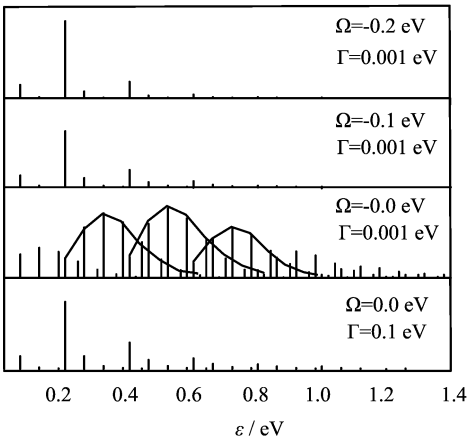

FIG. 5 The RRS spectrum of two mode model for narrow band excitation γ=0. The bars show the peak intensities $\sigma_{\nu_f}=|F_{\nu_f}|^2$. ω_{10}=0.2 eV, $\Delta Q_1/a_{10}$=2.07, ω_{20}=0.06 eV, $\Delta Q_2/a_{20}$=2.27.

ing gives a very convenient tool to purify the spectrum from the soft modes. The strong sensitivity of the RRS spectrum to the value of Γ indicates that an overestimation of the lifetime broadening (up to Γ≈0.1 eV) can give an incorrect spectral shape. Such a strong sensitivity can be used also in the estimations of Γ using the comparison of the theoretical and experimental spectra.

Now let us turn to the Raman spectra of real molecular systems. We study here the absorption and Raman spectra of two typical molecules guanine-cytosine (G-C) Watson-Crick base pairs and *trans*-1,3,5-hexatriene (THT) (Fig.6). The calculations of the RRS cross section for polyatomic molecules are computationally demanding in comparison with photoabsorption, because of the existence of numerous intermediate vibrational states. The problem of these intermediate states is eliminated in the time-dependent theory of the RRS

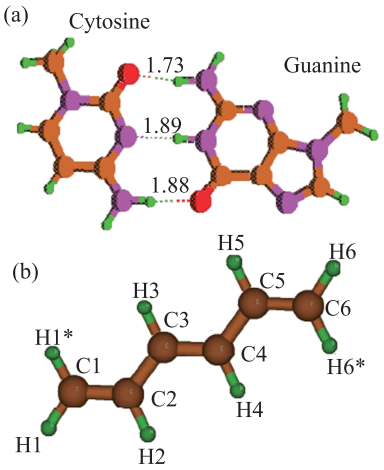

FIG. 6 The molecule structure of the guanine-cytosine (G-C) Watson-Crick base pairs (DNA) (a) and the *trans*-1,3,5-hexatriene (THT). The bond distance is in Å.

[18, 21, 54]. However, the solution of the time dependent Schrödinger equation on a multidimensional potential surface is also computationally expensive. The ST approximation bears with a significant numerical advantage for large molecules because it allows to avoid the calculations of excited state properties like gradients and vibrational frequencies. This method is applied for calculations of the RRS spectra of the DNA molecule. The good reasonable agreement with the experimental RRS spectra can here be referred to small HR parameters. The THT molecule is a representative of the systems where the ST approximation is limited. It should be noted that the response theory employed makes an implicit summation of the contributions of all excited states with varying, but typically large, Γ, while the theoretical analysis above is based on a two electronic level approximation, *i.e.* the ground and the resonant excited state.

C. DNA C-G base pair

Figure 6(a) displays the molecular structure of the GC base pair we obtained at the B3LYP/cc-PVDZ level. Our calculations show that the dimer hydrogen bond lengths (between cytosine and guanine) O−H, N−H, and H−O are 1.730, 1.890, and 1.880 Å, respectively, which is in good agreement with Sobolewski's theoretical results [55] based on the CC2 method. In another work, Sobolewski *et al.* investigated the low-lying excited singlet states using the *ab initio* multi-reference CASSCF method [56]. According to this calculation, there are three singlet excitations, one being a charge transfer excitation (CT) at 4.75 eV ($\pi_G\pi_C^*$) and two local excitations (LE) at 4.67 eV ($\pi_C\pi_C^*$) and 4.35 eV ($\pi_G\pi_G^*$). Our calculation at the B3LYP/cc-pVDZ level predicts the three lowest states with energies 4.53, 4.40,

DOI:10.1088/1674-0068/25/01/31-47

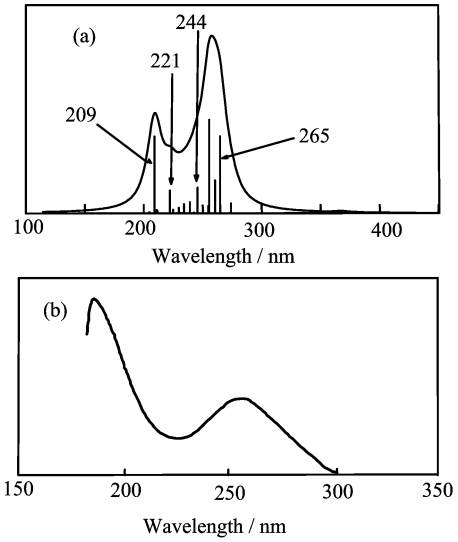

FIG. 7 UV Absorption spectra for the GS base pair DNA molecule. (a) The theoretical spectrum (gas phase) is based on the electronic oscillator strength distribution, broadened by Gaussian line profiles. (b) The experimental absorption spectrum [57].

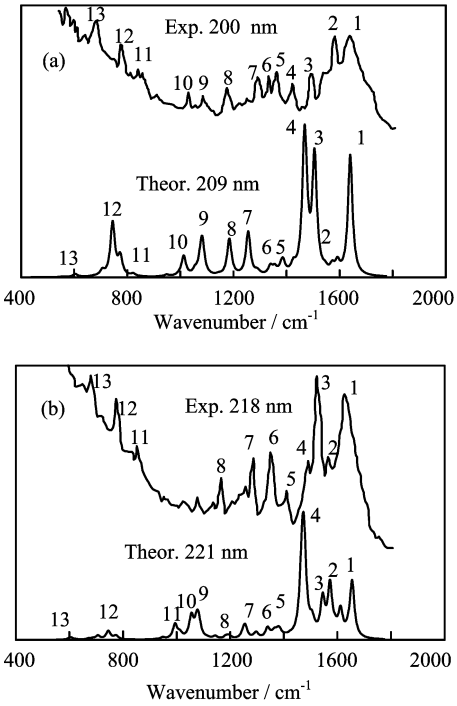

FIG. 8 Comparison of the theoretical and experimental Raman spectra [57] of the GS base pair DNA molecule for different excitation wavelengths. The spectra have been broadened by a Gaussian function with a width of γ=20 cm^{-1}.

and 3.40 eV. In our study the latter state (3.40 eV) is predicted to have a MG to MC charge transfer transition character, while according to the Sobolewski's work it should be a local excitation. However, this excited state is not involved in our Raman calculations.

The experimental UV absorption spectrum for the DNA base pair poly(dG-dC) in solution [57] is dominated by two broad structureless absorption peaks with a maximum at about 193 nm and a comparatively weak shoulder at around 260 nm (Fig.7). In the presentation of the theoretical spectrum we have included bars to represent the calculated oscillator strengths and provided a line profile obtained using a Gaussian line broadening. One can see that our theoretical UV absorption spectrum also displays two major peaks at 209 nm and about 260 nm, which are associated with significant oscillator strengths. However, the relative intensity of the two peaks is inverted in comparison with the experimental spectrum. The main reason for this discrepancy is that the experimental measurement and the theoretical calculation have been done in solution and gas phase, respectively, and that solvent effects can play a role in the assignment, in particular for charge-transfer transitions in the base pair. Another contributing reason could be a role of dispersion interaction [58, 59] which can not be properly handled using DFT theory.

Now let us turn to the Raman spectra under different excitation energies. Experimental resonant Raman spectra of the DNA base pair poly(dG-dC) in solution were measured in the work by Foder *et al.* for excitation wavelengths of 200–266 nm [57]. The spectra recorded at four different wavelengths, namely 200, 218, 240 and 266 nm, are included in Fig.8 and Fig.9. For comparison, we choose four calculated excitation frequencies as 209, 221, 244 and 265 nm, which are correlated to the highest oscillator strengths and are close to the experimental excitation wavelengths. In Fig.8(a) we present the calculated and experimental resonant Raman spectrum at 209 and 200 nm, respectively. More details of the theoretical and experimental frequencies in the region 400−2000 cm^{-1} are collected in Table I. It is clear from Fig.8(a) and Table I that the positions of the spectral features in general are very similar, while the relative intensities are different in the two spectra. The main difference between them is the peak at 1465 cm^{-1} (peak 4) which is found to be the strongest one in the calculated spectrum, while being relatively weak in the experimental spectrum. Furthermore, the peak around 1595 cm^{-1} (peak 2) is among the weakest peaks predicted by the theory whereas this is among the strongest peaks in the experimental spectrum. In Fig.10 we display the vibrational motion of the first four normal modes, namely those at 1642 cm^{-1} (peak 1), 1595 cm^{-1} (peak 2), 1507 cm^{-1} (peak 3), and 1465 cm^{-1} (peak 4) in theoretical spectrum. Although, the motions along those modes are delocalized, most of them can be assigned to different groups related to the hydrogen bonds. On the other hand, when the calculated excitation frequency is tuned to 221 nm (see Fig.8(b)), the shape and position of the spectrum becomes rather different for most of the peaks, particu-

DOI:10.1088/1674-0068/25/01/31-47

TABLE I Theoretical and experimental [57] frequencies (cm^{-1}) for Watson–Crick base pairs DNA (guanine–cytosin) at different excitation wavelengths.

Peak	Frequency[a]		Frequency[b]		Frequency[c]		Frequency[d]	
	Theory	Experiment	Theory	Experiment	Theory	Experiment	Theory	Experiment
1	1642	1632–1710	1610–1656	1632	1642	1632	1628–1671	1632
2	1595	1577	1575	1577	1571–1612	1577	1561	1577
3	1507	1489	1542	1528	1544	1528	1522	1528
4	1465	1419	1475	1489	1505	1489	1485, 1493	1489
5	1387	1364	1385	1419	1412–1428	1419	1424	1419
6	1342	1353	1344	1364	1381	1364	1381	1364
7	1261	1249	1299	1294	1340	1335	1319	
8	1189	1179	1187	1179	1301	1319	1269	
9	1083	1086	1144		1250		1209	
10	1016	1033	1077		1083		1052	
11	820	862.0	995		995	862	1067	
12	748–775	782.0	746	782	822	862	1022	
13	705	682.0	609	682	748	782	752	

[a] Experiment at 200 nm, theory at 209 nm.
[b] Experiment at 218 nm, theory at 221 nm.
[c] Experiment at 240 nm, theory at 244 nm.
[d] Experiment at 266 nm, theory at 265 nm.

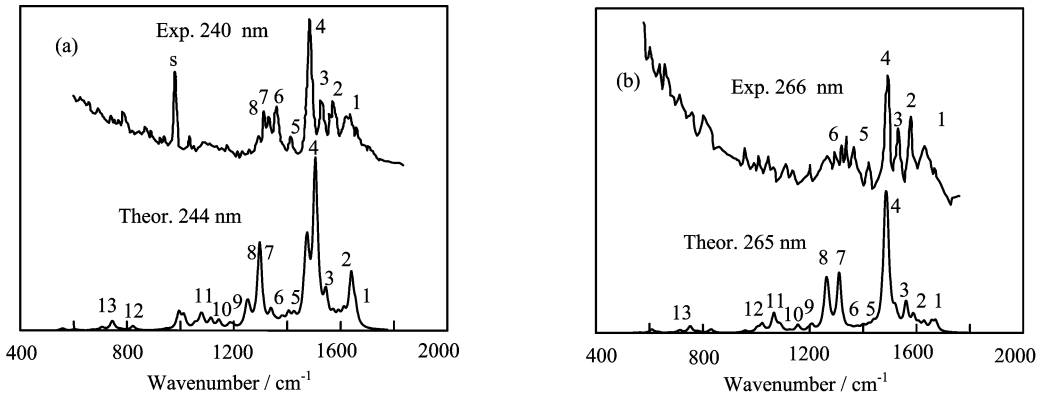

FIG. 9 Comparison of the theoretical and experimental Raman spectra [57] of the GS base pair DNA molecule for different excitation wavelengths. The spectra have been broadened by a Gaussian function with a width of γ=20 cm^{-1}.

larly for peaks 1, 3, 7, 8, and 12, the relative Raman intensity becomes lower compared to the spectrum obtained at 209 nm (Fig.8(a)). We note that, similar as the calculated spectra, the position and shape of the experimental spectrum also become different when we tune from 200 nm to 218 nm (Fig.8). The noticeable changes in the Raman intensity can be found around 1577 cm^{-1} (peak 2) and 1489 cm^{-1} (peak 3). Moreover, when the excitation energy is tuned to the next two lowest excited states (theory 244 nm, experiment 240 nm in Fig.9(a)) and (theory 265 nm, experiemt 266 nm in Fig.9(b)), the scattering intensities are dominated by the peak around 1500 cm^{-1} (peak 4), just as in the experimental spectra. With respect to the prediction of intensities for the fingerprint peaks, we find the agreement between theory and experiment to be satisfactory.

D. THT: A system with Large Huang-Rhys parameters

As a molecule for testing of theory we choose THT which has a well separated and well investigated excitation spectrum. Our calculations show that the optimized equilibrium structure of THT belongs to the C_{2h} point group with $\angle$ C_1–C_2–C_3, $\angle C_2$–C_3–C_4, C_1–C_2 distance, C_2–C_3 distance, and C_3–C_4 distance being equal to 122.5°, 124.3°, 1.345 Å, 1.452 Å, and 1.355 Å, respectively (see Fig.6). The agreement with the experimental structure reference data [60] is very good. However, since our calculations are concerned with Raman pa-

DOI:10.1088/1674-0068/25/01/31-47

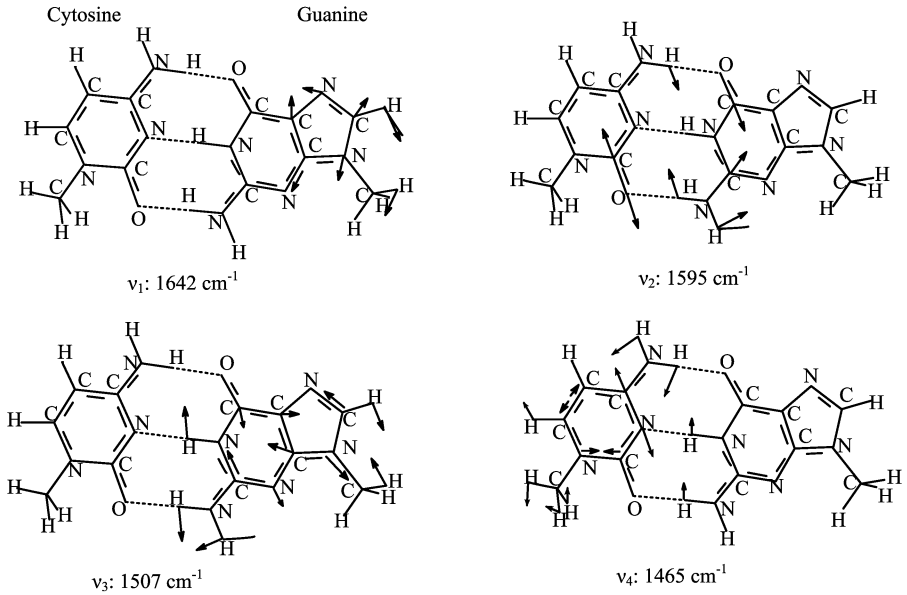

FIG. 10 The picture of more active vibrational modes of GS base pair DNA molecule.

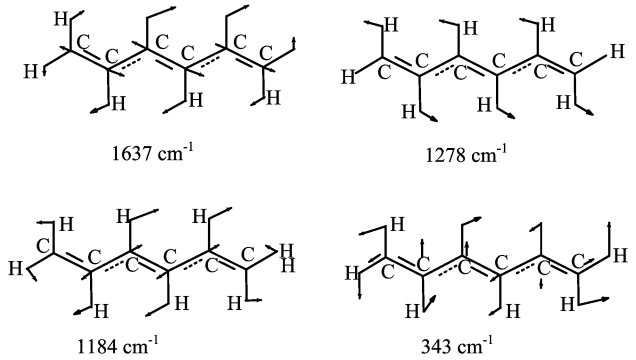

FIG. 11 The picture of more active vibrational modes of the *trans*-1,3,5-hexatriene molecule.

rameters, it becomes equally important to establish the quality of the force field, and, for that reason we compare our harmonic vibrational frequencies to the experimental fundamental frequencies observed in the resonant Raman spectrum reported by Myers and Pranta [29]. The experimental fundamental frequencies of the symmetric C=C stretch, symmetric C−H, symmetric =C–H stretch and symmetric C−C−C bend are 1635, 1295, 1192 and 354 cm^{-1}, respectively, while our corresponding theoretical harmonic frequencies are 1637, 1278, 1184 and 343 cm^{-1}, respectively (see Table II and Fig.11). We can thus conclude that our theoretical harmonic force field agrees very well with the experimental data.

The experimental UV absorption spectrum of THT in gas phase has been observed and presented by Myers *et al.* in the region between ca. 230−270 nm (see Fig.12) [29]. It is worthwhile to note that the absorption transition $(S_0)1^1A_g^- \rightarrow (S_1)2^1A_g^-$ is forbidden because of the

TABLE II Theoretical and experimental [29] frequencies (cm^{-1}) of the THT molecule with the symmetry of a_g.

mode	Frequency		Mode description
	Calc.	Exp	
ν_5	1637	1635	C=C, in the plane str.
ν_9	1278	1295	CH, rock
ν_{10}	1184	1192	=C–H, in the plane str.
ν_{13}	343	354	CCC, in plane bend

inversion symmetry. This transition though becomes allowed due to the vibronic coupling with the bright $1^1B_u^+$ state. The experimental spectrum which corresponds to the $1^1A_g^- \rightarrow 1^1B_u^+$ transition shows two strong bands and one medium strong band. Here we ignore the high excitation energies where the vibronic coupling between the symmetry allowed $1^1B_u^+$ and symmetry forbidden $2^1A_g^-$ states are important. Our calculation based on the CAMB3LYP/dau-cc-PVTZ level predicts only one single dominant electronic state, the one due to the transition $1^1A_g^- \rightarrow 1^1B_u^+$ with an energy of 4.860 eV and oscillator strength of 0.982.

The published information about the order of the dark $2^1A_g^-$ and bright $1^1B_u^+$ states at the equilibrium is rather controversial. According to experimental data the $1^1B_u^+$ state has lower energy (about 0.28/0.08 eV) [61−63]. The simulations based on the B3LYP functional with the cc-pVTZ basis set [64] and our CAMB3LYP/daug-cc-PVTZ calculations result in too high energy of the dark state with a gap about $\Delta = E(2^1A_g^-) - E(1^1B_u^+) \approx 2.27$ and 1.256 eV, respectively. The higher level of simulations based on the BHLYP functional [64] and the MRCI/DFT calcula-

DOI:10.1088/1674-0068/25/01/31-47

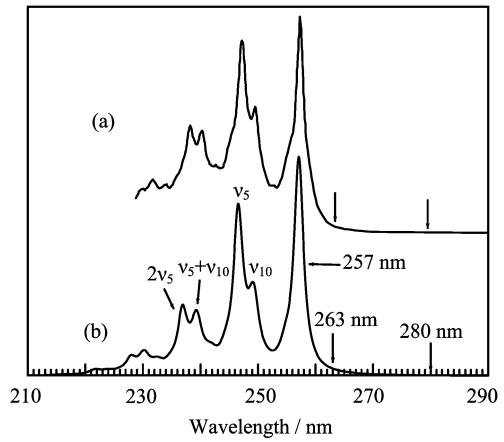

FIG. 12 Absorption spectrum of the THT molecule. (a) The experimental spectrum [29] blue shifted by $\Delta\lambda$=6 nm to match the theoretical spectrum. (b) The theoretical spectrum is calculated according to the linear coupling model (LCM) and Γ_{abs}=0.122 eV [29].

tions using the TZVVP basis set [65] give $\Delta=-0.03$ and -0.04 eV, respectively. Similar to the experimental data these calculations show that the discussed states are almost degenerate. The results based on the CASSCF/CASPT2/cc-pVTZ calculations [52, 66], on other hand, display the opposite trend $\Delta\approx-0.9$ eV. Nevertheless this uncertainty in Δ, the VC between the $2^1A_g^-$ and bright $1^1B_u^+$ states is important when the photon frequency is tuned in the resonance region [52]. A recent work based on spin flip response theory by Rinkevicius *et al.* has explored the character and ordering of the excited states of THT and other *trans*-polyenes in great detail [64], and we refer readers for that work for a more exhaustive account of THT energy levels.

In our simulations vibronic coupling is neglected because our main aim is to understand the transformation of the RRS spectrum when the photon energy is tuned below the absorption resonance. In this case the vibronic coupling effect is suppressed because the scattering becomes faster [4−6, 38, 67]. The suppression of the VC effect with decrease of the excitation frequency is also supported by the jet absorption measurements presented in Ref.[61].

In order to reproduce fine structure of the experimental absorption spectrum of THT, we took into account vibrations using the conventional FC technique [6]. For comparison, we display the experimental and theoretical absorption spectra of THT together in Fig.12. The experimental spectrum (upper) has been blue shifted about 6 nm to fit with the calculated spectrum (lower). One can see that the prediction of the relative absorption intensities shows a compelling overall agreement between the two spectra. We note that, just as in the experimental spectrum, there are two dominating bands, around 257 and 246 nm as a result of the 0-0 and 0-1 transitions, respectively. The latter one corresponds to a symmetric mode ν_5 (C=C, see Table II) which contributes strongly to the absorption spectrum. There are also one predicted medium strong band around 249 nm due to the 0-1 transition of the symmetric mode ν_{10} (=C–H), and two medium bands around 239 nm ($\nu_5+\nu_{10}$) and 237 nm ($2\nu_5$). It is obvious that the overtones and double-mode excitation give a significant contribution to the RRS spectra (see Fig.12).

The experimental resonance Raman spectra for THT in gas phase have also been recorded for 10 excitation wavelengths between 280 and 234 nm by Myers *et al.* [29]. The results have shown that due to the vibronic effects the overtone and combination bands contribute strongly to the spectra for some excitation frequencies. Using the same level of theory in the calculation of the absorption spectrum, we calculate the resonance and non-resonance Raman spectra for three different excitation frequencies, namely 257, 263, and 280 nm. The reason for this choice is partly that we want to study and define the short time approximation referring to excitations in the regions between those three resonance frequencies. Thus, our attention will mainly focus on the resonance and pre-resonance Raman scattering in the above mentioned excitation regions.

In Fig.13(a) we present the spectra of resonance Raman of THT using the gradient of the energy of the excited state (^1B_u) and the complex polarizability tensor calculated at 4.860 eV (255 nm). It is not surprising that the two spectra are identical, since there is a strong correlation between $\partial\alpha/\partial Q$ and the derivative of the excitation energy with respect to the normal mode coordinates. The theoretical and experimental spectra of THT for different excitation wavelengths at (theory 257 nm, experiment 251 nm), (theory 263 nm, experiment 257 nm) and (theory 286 nm, experiment 280 nm) are shown in Fig.13(b). In addition to the Raman profile for the fundamental (0-1), the overtone (0-2) and combination frequencies, we have also included the unshifted Raman scattering for the (0-0) transition, which is clearly dominant in the spectra. One can see that there is a very close agreement between theory and experiment (Fig.13(b)).

Noticeable differences exist between the resonant and off-resonant spectra, and the most noteworthy difference is that in the resonant case (257 and 263 nm) the intensities of the overtone ($2\nu_5$, around 3200 cm^{-1}) and combination modes ($\nu_5+\nu_{10}$, around 2800 cm^{-1}) are almost as high as that of the fundamental mode ν_{10}, while in the off-resonant case (280 nm), the overtone mode ($2\nu_5$) is completely depleted from the spectrum (because of the fast scattering). The similar behavior can clearly be seen in the experimental spectra (see Fig.13(b)). The collapse of the first and second overtones is clearly dependent on the shift between the ground and excited state potential surfaces, and accords with our discussion in the previous section.

DOI:10.1088/1674-0068/25/01/31-47

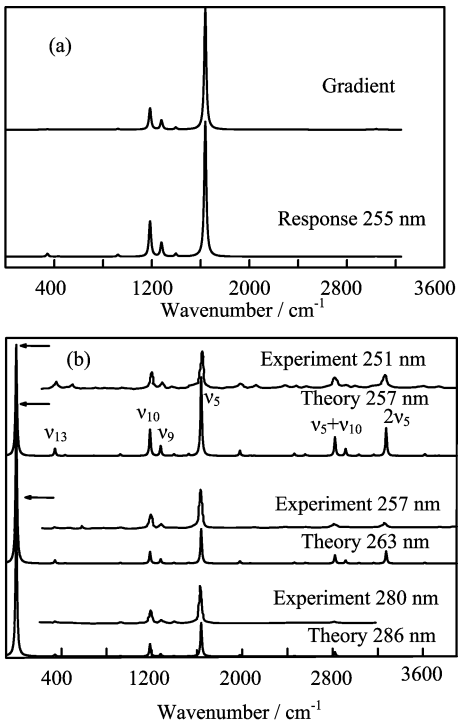

FIG. 13 (a) Resonance Raman spectra (at 255 nm) calculated according to the gradient of the potential surface of the excited state (upper) and short time approximation ST(Γ) (lower). (b) The theoretical and experimental [29] Raman spectra of the *trans*-1,3,5-hexatriene (C_6H_8) molecule for different excitation wavelengths. The theoretical calculation is based on linear coupling model (LCM). The spectra have been broadened by a Gaussian function with a width of γ=15 cm^{-1}. The experimental spectra were taken from Ref.[29].

VI. CONCLUSION

When vibrational frequencies are larger than the decay rate of the excited state, the nuclear wave packet spreads faster than the decay. This implicates that the short time approximation based on the assumption of a short lifetime of the intermediate state Γ^{-1} is not valid. In that case the short time approximation gives an incorrect dependence of the cross section on both photon frequency and Γ. Nevertheless, the spectral shape of the resonant Raman scattering can be obtained with reasonable accuracy when the displacements of excited state potentials from the ground state are small (small Huang-Rhys parameter). Quite often the deviation of the nuclear potential in the excited state from the ground state potential surface is significant and the role of the nuclear dynamics becomes important. This leads to the appearance of overtones in the Raman spectrum and to a strong variation of the spectral profile with respect to photon energy. The approximation based on an assumption about a short lifetime of the excited state, "the short-time approximation", is unable to describe these important effects.

In the present work we highlighted Raman scattering as a dynamical process with a finite duration time that results not only from the irreversible inhomogeneous broadening but also from the reversible dephasing of the scattering amplitude in the time domain. The latter mechanism makes the scattering fast when the photon energy is tuned from the absorption resonance. This constitutes a generalization of the short time approximation based solely on Γ, and provides a practical tool of controlling the scattering time and, hence, the nuclear dynamics using ordinary stationary measurements. Thus the short time limit can be reached easily by shortening of the scattering duration as it depends also on the detuning of photon frequency from the absorption band. To make the scattering fast it is sufficient to tune the photon frequency below the absorption band about one vibrational frequency. The shortened duration of the scattering implies a "purification" of the Raman spectrum by depleting higher overtones and soft vibrational modes, something that is exemplified by the here studied trans-1,3,5-hexatriene molecule. The low frequency modes are found to disappear faster when the RRS duration decreases. Such a frequency selective purification of the spectrum by the increase of detuning serves as a useful tool in assignments of spectra and greatly aids the interpretation of resonant Raman spectra of polyatomic molecules where a large number of overlapping vibrational resonances often make it difficult to analyse the experimental data.

The findings have important ramifications. Response theory offers a most versatile and rigorous theory of Raman scattering cross sections as it implicitly includes the full sum of intermediate states and gauge invariance, and, computationally, because it by now is implemented for all modern wave function or density functional models. Nevertheless, applicability of damped response theory for the complex polarizability at resonance will be dependent on the damping factor Γ and on the size of the Huang-Rhys parameter (if Γ is small). However, at detuned conditions this dependency disappears, and response theory becomes unconditionally applicable. Thereby it offers a most efficient determination of the Raman spectrum as it also avoids expensive calculations of potential energy surfaces of excited states. This in turn implies that by gradually stepping the detuning frequencies one can control Raman scattering for large molecules at elevated cross sections with purified fingerprinting and with fluorescence being quenched. This has an important bearing on the use of Raman scattering for stand-off detection of samples at ultra-low concentrations.

VII. ACKNOWLEDGMENTS

This work was supported by the Swedish Infrastructure Committee for the project "Multiphysics

DOI:10.1088/1674-0068/25/01/31-47

Modeling of Molecular Materials" (No.SNIC 023/07-18), the National Basic Research Program of China (No.2011CB808100), and the National Natural Science Foundation of China (No.10974121).

[1] L. L. Zhao, L. Jensen, and G. C. Schatz, Nano. Lett. **6**, 1229 (2006).
[2] L. Jensen, L. L. Zhao, and G. C. Schatz, J. Phys. Chem. C **12**, 4756 (2007).
[3] A. C. Albrecht, J. Chem. Phys. **34**, 1476 (1961).
[4] P. Skytt, P. Glans, J. Guo, K. Gunnelin, C. Såthe, J. Nordgren, A. Cesar, F. Gel'mukhanov, and H. Ågren, Phys. Rev. Lett. **77**, 5035 (1996).
[5] A. Cesar, F. Gel'mukhanov, Y. Luo, H. Ågren, P. Skytt, P. Glans, J. Guo, K. Gunnelin, and J. Nordgren, J. Chem. Phys. **106**, 3439 (1997).
[6] F. Gel'mukhanov and H. Ågren, Phys. Rep. **312**, 91 (1999).
[7] L. Jensen, L. L. Zhao, J. Autschbach, and G. C. Schatz, J. Chem. Phys. **123**, 174110 (2005).
[8] L. Jensen and G. C. Schatz, J. Phys. Chem. A **110**, 5973 (2006).
[9] J. Guthmuller and B. Champagne, J. Chem. Phys. **127**, 164507 (2007).
[10] E. J. Heller, R. Sundberg, and D. Tannor, J. Phys. Chem. **86**, 1822 (1982).
[11] H. Mohapatra and S. Umapathy, Chem. Phys. Lett. **390**, 427 (2004).
[12] B. Mennucci, C. Cappelli, R. Cammi, and J. Tomasi, Theor. Chem. Acc. **117**, 1029 (2007).
[13] M. Puranik, J. Chandrasekhar, J. G. Snijders, and S. Umapathy, J. Phys. Chem. A **105**, 10562 (2001).
[14] P. Salek, A. Baev, F. Gel'mukhanov, and H. Ågren, Phys. Chem. Chem. Phys. **5**, 1 (2003).
[15] T. Petrenko and F. Neese, J. Chem. Phys. **127**, 164319 (2007).
[16] A. Mohammed, H. Ågren, and P. Norman, Chem. Phys. Lett. **468**, 119 (2009).
[17] A. Mohammed, H. Ågren, and P. Norman, Phys. Chem. Chem. Phys. **11**, 4539 (2009).
[18] F. K. Gel'mukhanov, L. N. Mazalov, and A. V. Kondratenko, Chem. Phys. Lett. **46**, 133 (1977).
[19] F. Gel'mukhanov and H. Ågren, Phys. Rev. A **49**, 4378 (1994).
[20] Y. Luo, H. Ågren, F. Gel'mukhanov, J. Guo, P. Skytt, N. Wassdahl, and J. Nordgren, Phys. Rev. B **52**, 14479 (1995).
[21] P. Sałek, F. Gel'mukhanov, and H. Ågren, Phys. Rev. A **59**, 1147 (1999).
[22] T. Privalov, F. Gel'mukhanov, and H. Ågren, Phys. Rev. B **64**, 165116 (2001).
[23] F. Gel'mukhanov, P. Sałek, T. Privalov, and H. Ågren, Phys. Rev. A **59**, 380 (1999).
[24] H. Ågren, F. Gel'mukhanov, and P. Sałek, J. Jpn. Soc. Synchrotron Radiation **12**, 257 (1999).
[25] F. Gel'mukhanov, T. Privalov, and H. Ågren, Phys. Rev. A **56**, 256 (1997).
[26] K. A. Kane and L. Jensen, J. Phys. Chem. C **114**, 5540 (2010).
[27] D. Imre, J. L. Kinsey, A. Sinha, and J. Krenos, J. Phys. Chem. **88**, 3956 (1984).
[28] W. E. Smith and G. Dent, *Modern Raman Spectroscopy*, London: Willey and Sons, (2005).
[29] A. B. Myers and K. S. Pranata, J. Phys. Chem. **93**, 5079 (1989).
[30] C. M. Jones and S. A. Asher, J. Chem. Phys. **89**, 2649 (1988).
[31] E. V. Efremov, F. Ariese, A. J. G. Mank, and C. Gooijer, Anal. Chem. **78**, 3157 (2006).
[32] H. A. Kramers and W. Heisenberg, Zeitschrift für Physik **31**, 681 (1925).
[33] V. B. Berestetskii, E. M. Lifshitz, and L. P. Pitaevskii, *Quantum Electrodynamics Course of Theoretical Physics*, Vol. IV, Oxford: Butterworth-Heinemann, (1982).
[34] F. Gel'mukhanov, P. Sałek, A. Shalagin, and H. Ågren, J. Chem. Phys. **112**, 5593 (2000).
[35] F. F. Guimarães, V. Kimberg, V. C. Felicíssimo, F. Gel'mukhanov, A. Cesar, and H. Ågren, Phys. Rev. A **72**, 012714 (2005).
[36] H. Kleinert, *Path Integrals in Quantum Mechanics, Statistics, Polymer Physics, and Financial Markets*, London: World Scientific Publishing Co. Pte. Ltd., (2006).
[37] S. Sundin, F. Kh. Gel'mukhanov, H. Ågren, S. J. Osborne, A. Kikas, O. Björneholm, A. Ausmees, and S. Svensson, Phys. Rev. Lett. **79**, 1451 (1997).
[38] F. Hennies, S. Polyutov, I. Minkov, A. Pietzsch, F. Gel'mukhanov, M. Nagasono, L. Triguero, M. N. Piancastelli, W. Wurth, H. Ågren, and A. Föhlisch, Phys. Rev. Lett. **95**, 163002 (2005).
[39] M. Simon, L. Journel, R. Gullemin, W. C. Stolte, I. Minkov, F. Gel'mukhanov, P. Sałek, S. Carniato, R. Taïeb, A. C. Hudson, and D. W. Lindle, Phys. Rev. A **73**, 020706(R) (2006).
[40] J. C. Liu, C. Nicolas, Y. P. Sun, R. Flammini, P. O'Keeffe, L. Avaldi, P. Morin, V. Kimberg, N. Kosugi, F. Gel'mukhanov, and C. Miron, J. Phys. Chem. B **115**, 5103 (2011).
[41] F. Gel'mukhanov, T. Privalov, and H. Ågren, Sov. Phys. JETP **85**, 20 (1997).
[42] T. Privalov, F. Gel'mukhanov, and H. Ågren, Phys. Rev. B **59**, 9243 (1999).
[43] V. C. Felicíssimo, I. Minkov, F. F. Guimarães, F. Gel'mukhanov, A. Cesar, and H. Ågren, Chem. Phys. **312**, 311 (2005).
[44] T. H. Dunning Jr., J. Chem. Phys. **90**, 1007 (1989).
[45] Dalton, *A Molecular Electronic Structure Program*, Release 2.0 (2005), http://www.kjemi.uio.no/software/dalton/dalton.html.
[46] A. D. Becke, J. Chem. Phys. **98**, 5648 (1993).
[47] C. Lee, K. H. Park, M. Cho, W. T. Yang, and R. G. Parr, J. Chem. Phys. **125**, 114508 (2006).
[48] B. Miehlich, A. Savin, H. Stoll, and H. Preuss, Chem. Phys. Lett. **157**, 200 (1989).
[49] S. H. Vosko, L. Wilk, and M. Nusair, Can. J. Phys. **58**, 1200 (1980).
[50] T. Yanai, D. P. Tew, and N. C. Handy, Chem. Phys. Lett. **393**, 51 (2004).
[51] N. J. Turro, *Molecular Photochemistry*, New York: Benjamin, (1967).
[52] C. Woywod, W. C. Livingood, and J. H. Frederick, J.

DOI:10.1088/1674-0068/25/01/31-47

Chem. Phys. **112**, 626 (2000).
[53] R. Feifel, V. Kimberg, A. Baev, F. Gel'mukhanov, H. Ågren, C. Miron1, G. Öhrwall, M. N. Piancastelli, S. L. Sorensen, L. Karlsson, and S. Svensson, Phys. Rev. A **70**, 032708 (2004).
[54] G. Stock and W. Domcke, Adv. Chem. Phys. **100**, 1 (1997).
[55] A. L. Sobolewski, W. Domcke, and C. Hättig, PNAS **102**, 17903 (2005).
[56] A. L. Sobolewski and W. Domcke, Phys. Chem. Chem. Phys. **6**, 2763 (2004).
[57] S. P. A. Fodor and T. G. Spiro, J. Am. Chem. Soc. **108**, 3198 (1986).
[58] C. T. Lee, W. T. Yang, and R. G. Parr, Phys. Rev. B **37**, 785 (1988).
[59] L. Jensen and N. Govind, J. Phys. Chem. Lett. **113**, 9761 (2009).
[60] M. Traetteberg, Acta Chem. Scand. **22**, 2 (1968).
[61] D. G. Leopold, R. D. Pendley, J. L. Roebber, R. J. Hemley, and V. Vaida, J. Chem. Phys. **81**, 4218 (1984).
[62] W. M. Flicker, O. A. Mosher, and A. Kuppermann, Chem. Phys. Lett. **45**, 492 (1977).
[63] R. Mcdiarmid, Adv. Chem. Phys. **110**, 177 (1999).
[64] Z. Rinkevicius, O. Vahtras, and H. Ågren, J. Chem. Phys. **133**, 114104 (2010).
[65] C. M. Marian and N. Gilka, J. Chem. Theory Comput **4**, 1501 (2008).
[66] C. Woywod, W. C. Livingood, and J. H. Frederick, J. Chem. Phys. **112**, 613 (2000).
[67] F. Hennies, S. Polyutov, I. Minkov, A. Pietzsch, M. Nagasono, H. Ågren, L. Triguero, M. N. Piancastelli, W. Wurth, F. Gel'mukhanov, and A. Föhlisch, Phys. Rev. A **76**, 032505 (2007).

DOI:10.1088/1674-0068/25/01/31-47